A Low-Loss and Broadband MMI-Based Multi/Demultiplexer in Si_3N_4/SiO_2 Technology

Jinfeng Mu, Sergio A. Vázquez-Córdova, Mustafa Akin Sefunc, Yean-Sheng Yong, and Sonia M. García-Blanco, *Member, IEEE*

***Abstract*—A low-loss and broadband multimode interference (MMI)-based wavelength multi/demultiplexer in Si_3N_4/SiO_2 technology for erbium-doped lasing and amplifying applications is presented. The structural parameters of a 2 × 1 Si_3N_4 MMI multi/demultiplexer are optimized to minimize losses. The design and analysis of the MMI multi/demultiplexer are carried out using a hybrid approach, which combines a modified effective index method, the 2D film mode matching method, and the 2D beam propagation method, with lower impact in the computing requirements and simulation time than 3D methods. Simulated total losses of 0.19 and 0.23 dB at 980 and 1550 nm, respectively were obtained for the optimized MMI multi/demultiplexer. The measurements of our fabricated couplers, with 110 nm thick Si_3N_4 layer, show good agreement with our design. As multiplexers, the average losses of the MMI were measured to be 0.4 ± 0.3 dB for both 976 and 1550 nm wavelengths, and less than 1 dB across the whole C-band. As demultiplexers, the measured average extinction ratio of the fabricated MMI was found to be 21.4 ± 1.2 and 26.3 ± 0.8 dB for pump and signal wavelengths, respectively.**

***Index Terms*—Beam propagation and laser couplers, integrated optoelectronics, multi/demultiplexer, multimode interference (MMI), silicon nitride (Si_3N_4).**

I. Introduction

Stoichiometric silicon nitride (Si_3N_4) layers grown by low-pressure chemical vapor deposition (LPCVD) on oxidized silicon wafers have properties such as ultra-low propagation loss (0.1 dB/m at 1550 nm), high refractive index contrast, and large transmission window extending from ∼400 to 2350 nm [1]. Such attributes make the Si_3N_4/SiO_2 platform a promising candidate for the hybrid integration with other platforms such as silicon-on-insulator (SOI) [2] and rare-earth ion doped platforms [3]–[5]. The high refractive index contrast in comparison with the SiO_2/Si or polymer platforms leads to compact devices. The large transparency window is ideally suited to allow for the simultaneous propagation of the widely spectrally separated pump and signal fields typically used in rare-earth doped devices (i.e., 808/1064 nm for Nd^{3+}, 980/1030 nm for Yb^{3+}, 980/1550 nm for Er^{3+}, 790/2000 nm for Tm^{3+}). The integration of rare-earth doped materials with the Si_3N_4 platform will enable the realization of lasers and amplifiers exhibiting properties such as narrow linewidth [6], high power [7], tunability [8] and high gain [9] capable of high bit rate amplification [10] not easily achievable with other types of gain material. Furthermore, the large spectral separation between the pump and signal required for the pumping of Er^{3+}-doped devices lies within the transparency window of the Si_3N_4 platform. Instead of externally combining the pump and signal wavelengths at the input of the active devices or splitting the residual pump from the amplified/emitted signal at the output of the chip [4], [11], an low-loss and broadband multi/demultiplexer is significantly beneficial for densely integrated hybrid devices.

The most common device structures that have been proposed for combining and splitting different wavelengths include directional couplers (DC) [2], [12], asymmetric Y-junctions [13]–[15], Mach–Zehnder interferometers (MZI) [16], and multimode interference (MMI) devices [17]–[19]. Amongst them, directional couplers are very sensitive to fabrication errors, while the devices based on asymmetric Y-branches and MZI's are typically long and exhibit relatively high insertion losses (i.e., >1 dB). MMI-based devices can produce compact, low loss wavelength multi/demultiplexers with higher tolerance to fabrication errors than directional couplers. Many MMI designs have been implemented in the SOI platform to achieve tunable splitting ratios [20], [21], low-loss (∼0.2 dB) [22] and compact [23], [24] devices. A dual-channel MMI multiplexer with silicon oxynitride (SiON) core [25] was simulated to have signal (1550 nm) and pump (980 nm) losses of 0.28 and 0.63 dB respectively, nevertheless it had a large span with the device length of ∼2.5 mm. Comparing to SOI platforms, the work on MMI based on Si_3N_4 platforms is limited.

Different numerical methods, such as the vectorial beam propagation method (BPM), the finite-difference time-domain method, the eigenmode expansion method (EME) and the finite-element mode propagation analysis have been typically used for designing MMI couplers [26]–[28]. The implementation of these methods in three-dimensions (3D) usually provides higher simulation accuracy in comparison with the 2D counterpart, especially when the structures have wide propagation angles and large refractive index contrast.

However, the main disadvantages of 3D simulations are time and memory requirements, leading to excessive computation cost for the optimization of the MMI multi/demultiplexer, which involves multiple design parameters, such as port widths and locations. The effective index method (EIM) is typically used to convert the 3D structures [29] to 2D planar structures with

Manuscript received November 05, 2015; revised February 25, 2016; accepted June 03, 2016. Date of publication June 07, 2016; date of current version July 21, 2016. This work was supported by the "Stichting voor de Technisch Wetenschappen" (STW) under the project numbers STW-12832 and STW-13536.

The authors are with Optical Sciences Group, MESA+ Institute of Nanotechnology, University of Twente, 7500 AE Enschede, The Netherlands (e-mail: j.mu@utwente.nl; s.a.vazquezcordova-1@utwente.nl; m.a.sefunc@utwente.nl; y.s.yong@utwente.nl; s.m.garciablanco@utwente.nl).

Color versions of one or more of the figures in this paper are available online at http://ieeexplore.ieee.org.

Digital Object Identifier 10.1109/JLT.2016.2578463

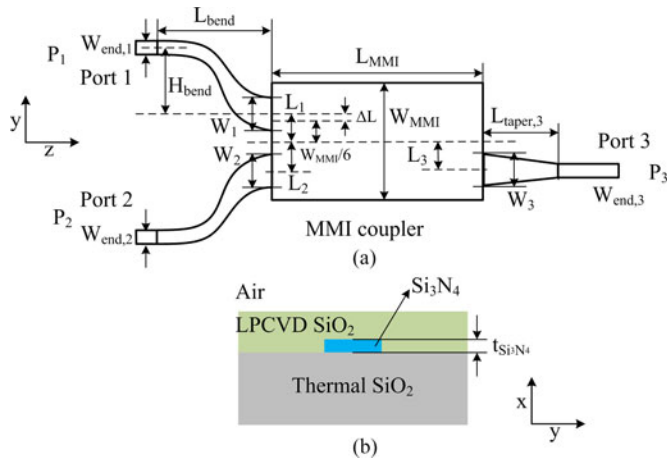

Fig. 1. (a) Schematic top view of the proposed MMI coupler. Input and output ports are tapered with $W_{\mathrm{end},i} = 1\ \mu\mathrm{m}$ $(i = 1, 2, 3)$. (b) Cross-section of the buried MMI coupler.

calculated effective indices. However, the effective indices of regions where no mode exists are not accurate enough for precision applications [30], such as for the estimation of the field patterns in the MMI with thin Si_3N_4 layer. Several approaches have been used to numerically modify the indices including the optimization of the cladding effective refractive index to achieve the same performance of the 3D model [27], and adjusting both cladding and core indices by comparing the results calculated with 2D and 3D simulations [31].

In this paper, a low-loss and broadband 2 × 1 Si_3N_4 MMI-based multi/demultiplexer with optimized structure is proposed to combine/split the 980 nm pump (λ_p) and 1550 nm signal (λ_s) for the hybrid integration of erbium-doped devices with the Si_3N_4 platform. A field mode matching (FMM) method, a modified EIM, and a fully vectorial 2D BPM are combined to achieve a fast and reliable optimization process. The designed MMI multi/demultiplexer theoretically exhibits total losses of 0.19 dB at 980 nm and 0.23 dB at 1550 nm. The MMI couplers were fabricated on 110 nm thick Si_3N_4 layer. As mutiplexer, the fabricated the MMI couplers show average losses of 0.4 ± 0.3 dB for both the 976 nm pump and the 1550 nm signal wavelengths. The losses of the optimal MMI coupler for the whole C-band were measured to be less than 1 dB. As demultiplexer, the average measured extinction ratios of the fabricated MMI are 21.4 ± 1.2 dB for the pump and 26.3 ± 0.8 dB for the signal. In both cases, the experimental results show good agreement with the simulations.

II. MMI Structure Design

A schematic structure of the proposed 2 × 1 MMI coupler is shown in Fig. 1(a). The cross-section of the waveguide structure is shown in Fig. 1(b). A dual-port, asymmetric, non-center fed design was selected as it allows for reversible operation (i.e., combiner in the left-right direction of Fig. 1(a) and divider in the right-left direction) with low insertion losses.

Tapered cosine S-bends are used to separate the input ports to match an input fiber array (i.e., 127 μm pitch), and a linear taper is employed for the output port. The ends of the tapers are connected to 1 μm wide straight waveguides in order to ensure single-mode propagation at the input/output of the device for both the pump and signal wavelengths. To maintain the adiabatic condition, both the length of the tapered cosine bends (L_{bend}) at the inputs of the MMI and the length of the linear taper ($L_{\mathrm{taper,3}}$) at its output are set to 800 μm, based on the result of simulations. The lateral distance between the center of the MMI and the center of each of its ports is denoted as L_{i} $(i = 1, 2, 3)$.

According to the self-imaging principle [32], the multiple confined modes in the multimode region of the MMI device interfere at the end of the structure producing single or multiple images of the launched field in the MMI. The field profile at position *L* along the propagation direction, *z*, can be expressed as the superposition of the field distributions of the different guided modes supported by the multimode region

$$\psi(y, L) = \sum_{v=0}^{m-1} c_v \psi_v(y) \exp\left[i \frac{v(v+2)\pi}{3L_\pi} L\right], \tag{1}$$

where *v* is the mode order, *m* is the number of modes supported by the multimode region, c_v is the modal excitation coefficient, *L* is the propagation distance of the field inside the MMI section, and L_π is beat length. L_π can be calculated as

$$L_\pi = \frac{\pi}{\beta_0 - \beta_1} \tag{2}$$

where β_0 and β_1 are the propagation constants of the two lowest order modes of the multimode region. The field profile, $\psi(y, L)$, is therefore determined by c_v and the phase factor. The modal excitation coefficients, c_{v} can be numerically calculated as the overlap integral between the fundamental mode of the input port and the *v*-th order mode of the MMI section. Self-imaging of the input field will take place at propagation distances $L = N(3L_\pi)$, where $N = 0, 1, 2 \ldots$, with direct images occurring for even *N* numbers and mirrored images for odd *N* numbers. If the remainder of $v(v+2)/3$ is equal to zero, paired interference is obtained. In this case, self-imaging can be realized at three times shorter propagation distances $[L = N(L_\pi)]$. Such excitation condition can be achieved if the lateral offset $(L_i, i = 1, 2, 3)$ is theoretically equal to one-sixth of the effective width of the MMI, which takes into account the penetration depth of the electromagnetic field into the cladding. In order for the MMI device to work in both directions as a coupler (forward direction) and a splitter (backward propagation direction) for the pump and signal wavelengths, the same values of L_i (i.e., $L_1 = L_2 = L_3$) are selected in the design.

For the MMI coupler depicted in Fig. 1(a) to work as a wavelength combiner, the length of the MMI section, L_{MMI}, should be selected so that a mirrored image is obtained from port 1 (i.e., 1550 nm signal, λ_s) to port 3 and a direct image is achieved from port 2 (i.e., 980 nm pump, λ_p.) to port 3. As discussed above, paired interference requires that the length of the MMI is selected as $L_{\mathrm{MMI}} = p(L_\pi^{\lambda_p})$ with *p* an even integer ($p = 2, 4, 6 \ldots$) to achieve a direct image for the pump and $L_{\mathrm{MMI}} = q(L_\pi^{\lambda_s})$ with *q* an odd integer ($q = 1, 3, 5 \ldots$) to obtain a mirrored image for the signal. Therefore, the length of

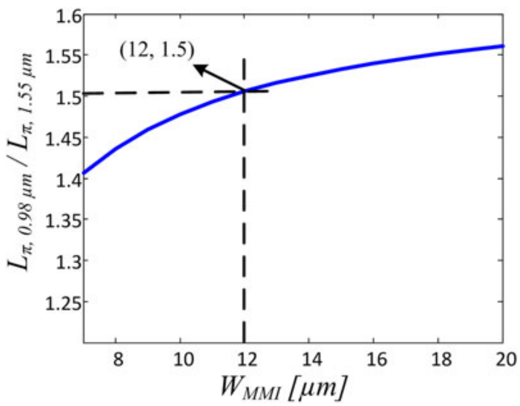

Fig. 2. Beat length ratio as a function of Si_3N_4 width.

the MMI should verify $L_{\mathrm{MMI}} = p\,(L_\pi^{\lambda_p}) = q(L_\pi^{\lambda_s})$ in order to work as a wavelength combiner/splitter for λ_p and λ_s.

III. Simulation Results

In this work, a hybrid design method including a FMM algorithm, followed by a modified EIM and 2D BPM is utilized to optimize a multi/demultiplexer in Si_3N_4/SiO_2 waveguide technology working for transverse-electric (TE) polarization. A 2D-BPM algorithm was chosen over the EME because it considers all the modes of the multimode MMI region while presenting a small advantage in simulation time.

As a first step, a 2D-FMM algorithm (FieldDesigner, PhoeniX B.V.) is utilized to select the width and length of the MMI region. The propagation constants of the different modes supported by MMI cross-sections of different widths (W_{MMI}) are calculated for both $\lambda_p = 980$ nm and $\lambda_s = 1550$ nm wavelengths. The beat lengths (L_π) for both signal and pump wavelengths are calculated using Eq. (2). The ratio of the beat lengths of pump and signal is then computed to determine the width of the MMI section. As discussed above, ${L_\pi}^{\lambda_p}/{L_\pi}^{\lambda_s} = q/p$ in order to achieve the correct direct (for the pump) and mirrored (for the signal) image at the output of the MMI, which is necessary to achieve a wavelength combiner.

Fig. 2 shows that for a thickness of the Si_3N_4 layer of 110 nm, a ratio of 1.5 (i.e., $p = 2$, $q = 3$) can be achieved for an MMI width of $\sim$12 μm, which supports 10 and 6 confined TE modes for 980 and 1550 nm, respectively. A ratio of 1.5 means that the input signal field will be mirrored and the pump input field will form a direct image after a propagation distance of 647 μm ($L = 2{L_\pi}^{\lambda_p} \approx 3{L_\pi}^{\lambda_s}$). Table I shows the refractive indices of the materials used in the simulations. The effective refractive indices of two lowest order modes of the MMI region as well as the resulting beat length are also shown.

Once the width and length of the multimode region of the MMI device have been fixed, the next step involves the use of a 2D-BPM algorithm (OptoDesigner, PhoeniX B.V.) to optimize the dimensions of the input and output ports as well as their exact locations. A modified EIM is employed in order to obtain reliable effective indices (n_{eff}) to be used for the core and cladding regions in the 2D BPM model.

TABLE I
Relevant Refractive Index Values Used in the Simulations

Wavelength (nm)	Material	n material (TE)	n_{eff} of two lowest TE modes	Beat length (μm) @ $W_{\mathrm{MMI}} = 12\ \mu$m
980	SiO_2	1.4492	1.5604	323.8
	Si_3N_4	1.9936	1.5589	
1550	SiO_2	1.4456	1.4957	215.7
	Si_3N_4	1.9835	1.4921	

n_{eff} of the two lowest order modes used to calculate the beat length. Device parameters: $W_{\mathrm{MMI}} = 12\ \mu$m, $L_{\mathrm{MMI}} = 647\ \mu$m, $t_{\mathrm{Si3N4}} = 110$ nm. TE Polarization.

TABLE II
Beat Lengths

Wavelength (nm)	980	1550
n_{core}	1.5609	1.4969
n_{clad}	1.3918	1.420
L_π (μm) ($W_{\mathrm{MMI}} = 4\ \mu$m)	40.26 (2D FMM)	33.46 (2D FMM)
	40.19 (EIM)	32.80 (EIM)
L_π (μm) ($W_{\mathrm{MMI}} = 8\ \mu$m)	147.99 (2D FMM)	103.44 (2D FMM)
	147.97 (EIM)	103.3 (EIM)
L_π (μm) ($W_{\mathrm{MMI}} = 12\ \mu$m)	323.8 (2D FMM)	215.68 (2D FMM)
	323.8 (EIM)	215.68 (EIM)
L_π (μm) ($W_{\mathrm{MMI}} = 20\ \mu$m)	879.32 (2D FMM)	564.25 (2D FMM)
	879.33 (EIM)	564.41 (EIM)

Comparison of beat lengths calculated using the 2D FMM and modified-EIM methods for various W_{MMI}. Device parameters: $t_{\mathrm{Si3N4}} = 110$ nm. TE Polarization.

In this work, the effective refractive index of the cladding, n_{clad}, is modified. The refractive index utilized for the core, n_{core}, is the 1D effective index of the $n_{SiO2}/n_{Si3N4}/n_{SiO2}$ stack. Our algorithm modifies n_{clad} until the respective beat lengths calculated with the EIM and 2D FMM converges. The convergence test is implemented in parallel for a number of Si_3N_4 core widths ranging from 4 to 20 μm. Table II shows a comparison of beat lengths calculated by the modified EIM and by FMM. The finally optimized refractive index values for the cladding region are 1.3918 at 980 nm and 1.420 at 1550 nm, which are used in the 2D BPM model for the optimization of the input and output ports as described in the following sections.

In order to investigate the influence of the width and location of each input port, only one input port is considered in each simulation. The input field is launched at the end of the tapered input port [i.e., port 1 for λ_s, and port 2 for λ_p, see Fig. 1(a)]. The loss of the MMI coupler is computed from the simulated power at the end of the tapered output port, P_3, as $-10 \times \log_{10}(P_3/P_{1,2})$. Figs. 3 and 4 show the simulated MMI losses (in dB) for different widths of the relevant port (i.e., $W_{1,2}$) and offset (ΔL) of the location of each port with respect to the "nominal" $W_{\mathrm{MMI}}/6$ for 980 nm pump and the 1550 nm signal wavelengths, respectively. ΔL is positive since the effective width (i.e., considering the penetration depth of the electromagnetic field into the cladding) is larger than the waveguide width W_{MMI}. As shown in both figures, the wider the input port, the lower the MMI losses for both wavelengths. Furthermore, as the width of the input port becomes larger, the range of offset values (ΔL) for which low losses are achieved increases. Multiple

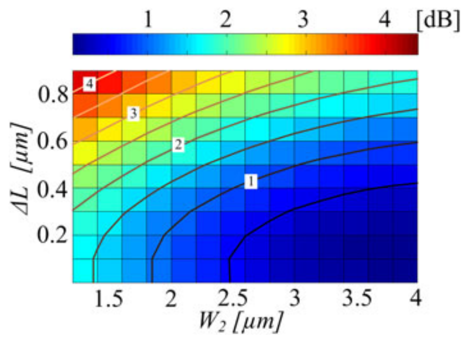

Fig. 3. MMI loss (in dB) for 980 nm pump through input port 2, as a function of port 2 width (W_2) and offset (ΔL) with respect to nominal location at W_{MMI}/6.

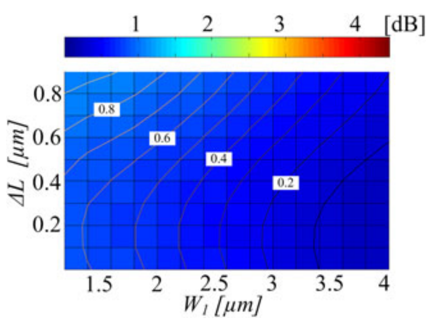

Fig. 4. MMI loss for 1550 nm signal through input port 1 as a function of port 1 width (W_1) and offset (ΔL) with respect to nominal location at W_{MMI}/6.

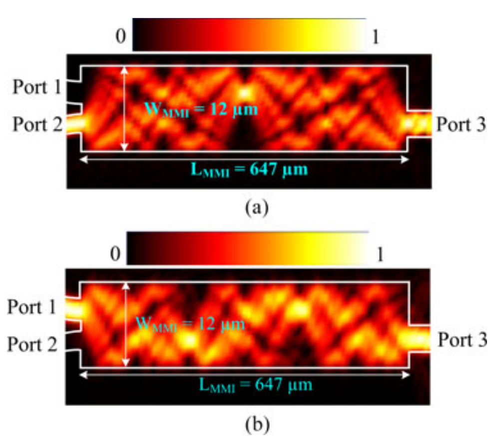

Fig. 5. (a) Field profile of the designed MMI coupler for 980 nm pump wavelength. (b) Field profile of the designed MMI coupler for 1550 nm signal wavelength. Device parameters: $W_{\mathrm{MMI}} = 12\ \mu$m, $L_{\mathrm{MMI}} = 647\ \mu$m, $W_1 = 3.6\ \mu$m, $W_2 = 3.0\ \mu$m, $W_3 = 4\ \mu$m and $\Delta L = 0.1\ \mu$m. TE polarization.

values of W_3 were investigated, from which $W_3 = 4\ \mu$m was found to have the best performance.

Cross-talk between the two input ports occurs as the distance between them decreases. The maximum values of W_1 and W_2 that avoid cross-talk were calculated using the 2D FMM method to be $W_1 < 3.8\ \mu$m and $W_2 < 3.2\ \mu$m. $W_1 = 3.6\ \mu$m, $W_2 = 3.0\ \mu$m, $W_3 = 4\ \mu$m and $\Delta L = 0.1\ \mu$m were adopted in the optimal design. The propagating fields in the optimal MMI coupler are displayed in Fig. 5(a) and (b), for pump and signal wavelengths respectively.

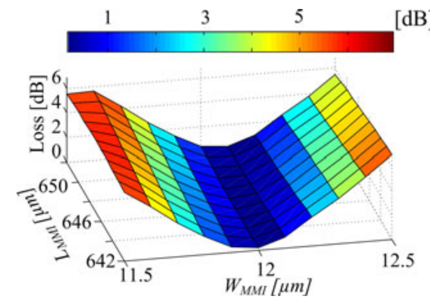

Fig. 6. Total MMI loss as a function of the optimal device length and width at 980 nm.

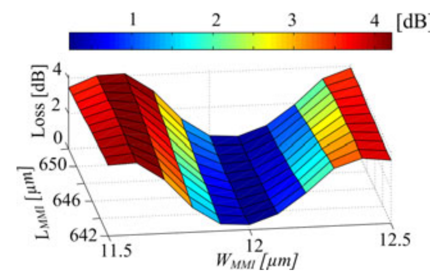

Fig. 7. Total MMI loss as a function of the optimal device length and width at 1550 nm.

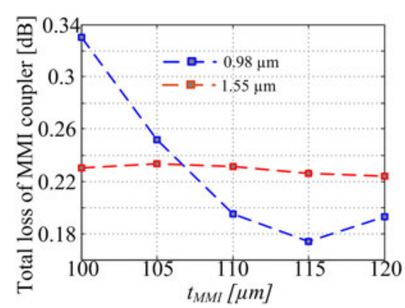

Fig. 8. Total MMI loss for ±10 nm variations of Si_3N_4 thickness for 980 μm and 1550 nm.

Prior to fabrication, the robustness of the design to fabrication errors was investigated by varying the different fabrication parameters such as the width and length of the MMI section, and the thickness of the Si_3N_4 layer. Figs. 6 and 7 show the loss of the device in dB as a function of both W_{MMI} and L_{MMI} for the pump and signal respectively. As seen from Figs. 6 and 7, the MMI coupler is more tolerant to changes of the length than to changes of the width for both pump and signal wavelengths.

Furthermore, the effect of the Si_3N_4 layer thickness variation on the total MMI loss is shown in Fig. 8. For a ±10 nm variation range, the total losses of the device are below 0.34 dB for both wavelengths. At the selected dimensions (i.e. 12 μm width, 647 μm length and 110 nm thickness), the simulated MMI losses are ~0.19 dB at 980 nm and ~0.23 dB at 1550 nm.

IV. Fabrication

Due to the high sensitivity of the performance of the device to variations of its width (W_{MMI}), the designed MMI width was varied from 11.5 μm to 12.5 in steps of 0.1 μm. The

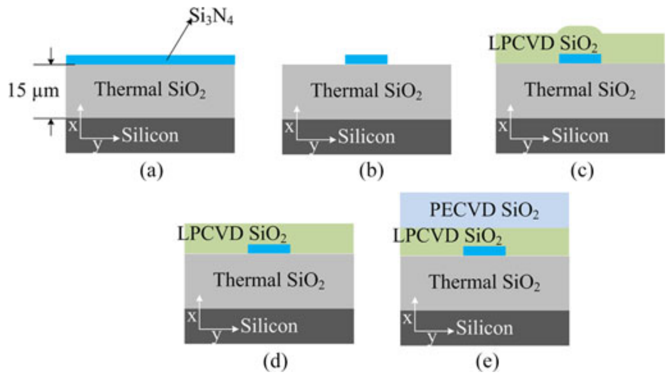

Fig. 9. Schematic of the waveguide fabrication process. (a) A 110 nm Si_3N_4 layer is deposited using LPCVD. (b) Waveguide structures are fabricated by conventional photolithography followed by RIE etching. (c) LPCVD SiO_2 is deposited on the top of the structure. (d) The surface is polished using CMP. (e) A SiO_2 layer is deposited using PECVD.

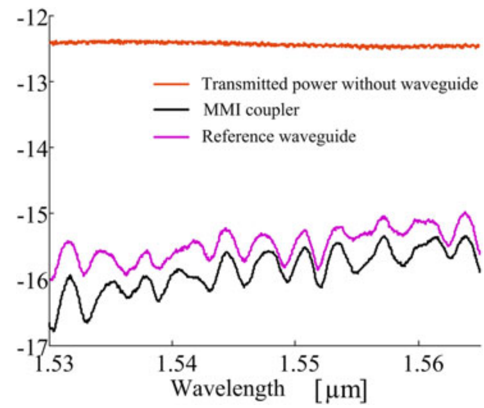

Fig. 10. Measured power without the chip, after MMI coupler (width 12 μm) and after reference straight waveguide (width 1 μm) besides the MMI coupler.

waveguides were fabricated using standard microfabrication process technology [33] as shown in Fig. 9.

Firstly, a 110 nm thick Si_3N_4 layer was deposited by LPCVD on a thermally oxidized silicon substrate with 15 μm of thermal oxide, which avoids leaking of the propagating TE_0 mode into the silicon substrate. The thickness of the LPCVD Si_3N_4 layers can be controlled to be within 5 nm. The measured thickness (Woollam M-20000UI ellipsometer) of the deposited Si_3N_4 layer was 112.4 $\pm$ 0.4 nm. The MMI structures were then patterned using lithography with vacuum contact mode, after which a reflow process was utilized in order to smooth the edges. Reactive ion etching (RIE) was used to fabricate the waveguide structure. The dimensions of the devices can be typically controlled to be $\pm$0.2 μm. However, the measured fabricated widths were about 0.3 μm smaller than the designed values. After etching, a layer of LPCVD SiO_2 ($\sim$200 nm thick) was deposited on the top of the waveguide as upper cladding. The wafer was annealed at about 1150 °C and gradually cooled down to room temperature ($\sim$20 °C) to avoid cracking. The protrusion of SiO_2 on the top was removed by chemical–mechanical polishing (CMP). A micrometer scale SiO_2 layer was further deposited by plasma enhanced chemical vapor deposition (PECVD) followed by the same annealing process.

The devices were diced perpendicularly (Loadpoint Micro Ace 3, Disco NBC-Z blade) to the input and output waveguides. No antireflection coating was applied to the end-facets.

V. Characterization

The fabricated MMI couplers were characterized in the C-band (1530-1565 nm) using a tunable laser (Agilent 8164B), and at 976 nm with a diode laser. A single mode polarization maintaining fiber (PM980-XP) was used to couple TE polarized light into the waveguides, since the devices under test are polarization sensitive and were designed to work for TE polarization. The waveguide output was coupled into a single-mode fiber (UHNA3) connected to a power meter. The width of the input/output Si_3N_4 waveguide is 1 μm, which only supports a single mode for both the pump and C-band wavelengths. The higher order modes of the tapered regions can be sufficiently suppressed during input/output coupling.

Fig. 10 shows the transmitted power in the C-band without the chip (~ -12.4 dBm), the output power after a reference straight-waveguide and the MMI coupler. The reference waveguide insertion loss, obtained by subtracting the system transmission in the C-band from the transmission of the reference waveguide, varies from $\sim$4.3 dB at 1530 nm to $\sim$3.7 dB at 1565 nm. The propagation loss of a single mode Si_3N_4 waveguide is $<$0.1 dB/cm. The reference waveguide propagation loss is therefore $<$0.05 dB. The insertion loss of the straight reference waveguide (1 μm width, 112 nm thick) placed next to the MMI structures is mainly caused by the mode mismatch between the input fiber and the waveguide, which introduces coupling losses. At 1550 nm, the mode field diameter of the input fiber is considered as 10 $\pm$ 0.5 μm and the one of the output fiber is 4.1 $\pm$ 0.3 μm. The total theoretical coupling losses caused by the mode mismatch between the input and output fibers and waveguides are calculated to be $\sim$3.9 dB. The measured reference waveguide insertion losses match very closely the calculated ones. The MMI coupler can be assumed to have the same input/output coupling loss as its neighboring reference waveguide. Therefore, the total loss of the MMI coupler was calculated by subtracting the insertion loss of the reference waveguide from the insertion loss of the MMI coupler [Fig. 11(a)]. Furthermore, some oscillations are visible in the transmission measurements of Fig. 10. The oscillations are almost identical for both the transmission measurements of the reference waveguide and MMI device. Their origin is therefore not from the device under test. When performing Fourier analysis on the transmission measurement of the system without chip, the same frequency component is found. The amplitude of the oscillations dramatically increases when introducing the device under test and they reduce when introducing a circulator prior to the chip The most probably origin of the oscillations is therefore back-reflections into the tunable laser cavity.

The total losses across the C-band of the MMI coupler with 12 μm width are shown in Fig. 11(a). The simulated losses are also plotted (dotted line). The total losses were 0.4 $\pm$ 0.3 dB at 1550 nm, and less than 1 dB for all wavelengths of the C-band. Fig. 11(b) and (c) show the total losses for pump and signal as a function of MMI width respectively. A good agreement between simulated and measured values can be seen. The MMI coupler

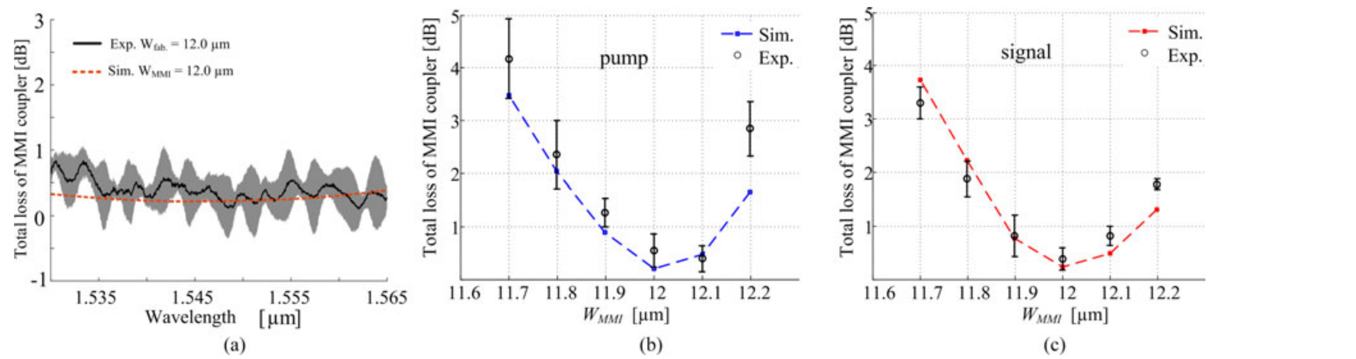

Fig. 11. (a) Total MMI losses of an MMI coupler across all C-band wavelengths ($W_{\mathrm{MMI}} = 12\ \mu\mathrm{m}$, $L_{\mathrm{MMI}} = 647\ \mu\mathrm{m}$, $t_{\mathrm{MMI}} = 112\ \mathrm{nm}$). Total MMI losses as a function of W_{MMI} at (b) 976 nm and (c) 1550 nm. Shadows depict measurement deviation.

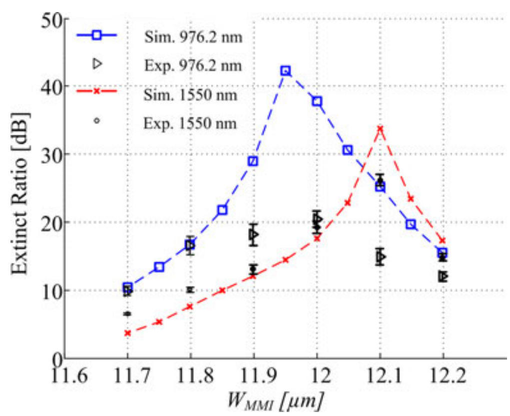

Fig. 12. A comparison of the measured and simulated ER (in dB) of the MMI couplers as a function of W_{MMI}.

is sensitive to variations of the width of the multimode region. In order to keep the device losses below 1 dB, the width of the multimode region should be controlled within $\pm 0.14\ \mu$m.

To estimate the performance of the MMI couplers working reversely as splitters, both λ_p and λ_s were launched into port 3 and the output fibers for pump and signal were aligned to the corresponding ports 2 and 1 respectively. When launching the pump into port 3, the transmitted power to both port 2 ($P_{2,p}$) and port 1 ($P_{1,p}$) were measured. In the same way, the signal power transmitted to both output ports, $P_{1,s}$ and $P_{2,s}$ were measured. Then the ER values for the pump and signal were calculated as $10 \times \log_{10}(P_{2,p}/P_{1,p})$ and $10 \times \log_{10}(P_{1,s}/P_{2,s})$ respectively.

A comparison between the experimental and simulated ERs is shown in Fig. 12. The maximum average ER value for the signal was 26.3 dB for the MMI at fabricated width of 12.1 μm while the maximum ER for the pump was 21.4 dB for the MMI with fabricated width 12.0 μm. The measured ER values are lower than the simulated ones, which are attributed to low levels of stray lights arriving to ports 1 and 2 respectively.

Furthermore, scattering due to imperfection in the propagation region of MMI could affect more on the pump than the signal due to the wavelength. Ideally, a series of cascaded MMIs should be characterized in order to obtain a more accurate ER value.

Since the proposed device is intended to be integrated with active devices, reflections of the MMI structure back to the active material could affect the performance of the active devices. Eigenmode expansion simulation package from Lumerical MODE was used to calculate the power reflected from the MMI structure. The reflection coefficient can be extracted from the s11 component of the scattering matrix. A power reflection coefficient was calculated to be $\sim 10^{-31}$, which can be negligible.

VI. Conclusion

A low-loss and broadband multi/demultiplexer for erbium-doped lasing and amplifying applications is presented. The 110 nm thick Si_3N_4 multi/demultiplexer is designed by combining the modified EIM, 2D-FMM and 2D-BPM methods, which avoids the time-consuming 3D simulations, and enables to determine an optimal MMI structure with restricted port configurations and variation multiple design parameters. The calculated losses of the optimal coupler were found to be 0.19 dB at 980 nm wavelength and 0.23 dB at 1550 nm. The characterization was carried out at 976 nm and at all wavelengths in the C-band. As combiners, the total losses of the MMI coupler were measured as 0.4 ± 0.3 dB for both pump and signal wavelengths, and less than 1 dB for all the other wavelengths in C-band. As splitters, the average extinction ratios were measured to be 21.4 and 26.3 dB for pump and signal respectively.

Acknowledgment

The authors would like to thank L. Chang, M. Hoekman, K. Wörhoff, R. Stoffer, and A. Leinse for their useful discussions.

References

[1] K. Wörhoff, R. G. Heideman, A. Leinse, and M. Hoekman, "TriPleX: A versatile dielectric photonic platform," *Adv. Opt. Technol.*, vol. 4, pp. 189–207, Apr. 2015.

[2] W. D. Sacher *et al.*, "Polarization rotator-splitters and controllers in a Si_3N_4-on-SOI integrated photonics platform," *Opt. Express*, vol. 22, pp. 11167–11174, May 2014.

[3] W. Lei, G. Ruimin, W. Bing, W. Xingjun, and Z. Zhiping, "Hybrid Si_3N_4-Er/Yb silicate waveguides for amplifier application," *IEEE Photon. Technol. Lett.*, vol. 24, no. 11, pp. 900–902, Jun. 2012.

[4] M. Belt and D. J. Blumenthal, "Erbium-doped waveguide DBR and DFB laser arrays integrated within an ultra-low-loss Si_3N_4 platform," *Opt. Express*, vol. 22, pp. 10655–10660, May 2014.

[5] M. Piels, J. F. Bauters, M. L. Davenport, M. J. R. Heck, and J. E. Bowers, "Low-loss silicon nitride AWG demultiplexer heterogeneously integrated with hybrid III-V/silicon photodetectors," *J. Lightw. Technol.*, vol. 32, no. 4, pp. 817–823, Feb. 2014.

[6] E. H. Bernhardi *et al*., "Ultra-narrow-linewidth, single-frequency distributed feedback waveguide laser in Al_2O_3:Er^{3+} on silicon," *Opt. Lett.*, vol. 35, pp. 2394–2396, Jul. 2010.

[7] K. van Dalfsen, S. Aravazhi, C. Grivas, S. M. García-Blanco, and M. Pollnau, "Thulium channel waveguide laser with 1.6 W of output power and ∼80% slope efficiency," *Opt. Lett.*, vol. 39, pp. 4380–4383, Aug. 2014.

[8] D. Geskus, S. Aravazhi, K. Wörhoff, and M. Pollnau, "High-power, broadly tunable, and low-quantum-defect $KGd_{1-x}Lu_x(WO_4)_2$:Yb^{3+} channel waveguide lasers," *Opt. Express*, vol. 18, pp. 26107–26112, Dec. 2010.

[9] D. Geskus, S. Aravazhi, S. M. García-Blanco, and M. Pollnau, "Giant optical gain in a rare-earth-ion-doped microstructure," *Adv. Mater.*, vol. 24, pp. OP19–OP22, Oct. 2012.

[10] J. D. B. Bradley *et al*., "170 Gbit/s transmission in an erbium-doped waveguide amplifier on silicon," *Opt. Express*, vol. 17, pp. 22201–22208, Nov. 2009.

[11] J. D. B. Bradley *et al*., "Monolithic erbium- and ytterbium-doped microring lasers on silicon chips," *Opt. Express*, vol. 22, pp. 12226–12237, May 2014.

[12] Y.-D. Yang, Y. Li, Y.-Z. Huang, and A. W. Poon, "Silicon nitride three-mode division multiplexing and wavelength-division multiplexing using asymmetrical directional couplers and microring resonators," *Opt. Express*, vol. 22, pp. 22172–22183, Sep. 2014.

[13] Z. Weissman, D. Nir, S. Ruschin, and A. Hardy, "Asymmetric Y-junction wavelength demultiplexer based on segmented waveguides," *Appl. Phys. Lett.*, vol. 67, pp. 302–304, Jan. 1995.

[14] D. Bucci, J. Grelin, E. Ghibaudo, and J.-E. Broquin, "Realization of a 980-nm/1550-nm pump-signal (de)multiplexer made by ion-exchange on glass using a segmented asymmetric y-junction," *IEEE Photon. Technol. Lett.*, vol. 19, no. 9, pp. 698–700, May 2007.

[15] L. Onestas, D. Bucci, E. Ghibaudo, and J. E. Broquin, "Vertically integrated broadband duplexer for erbium-doped waveguide amplifiers made by ion exchange on glass," *IEEE Photon. Technol. Lett.*, vol. 23, no. 10, pp. 648–650, May 2011.

[16] G. Zhang, S. Honkanen, A. Tervonen, C.-M. Wu, and S. I. Najafi, "Glass integrated optics circuit for 1.48/1.55-and 1.30/1.55-μm-wavelength division multiplexing and 1/8 splitting," *Appl. Opt.*, vol. 33, pp. 3371–3374, Jun. 1994.

[17] S. Singh *et al*., "An MMI-based wavelength combiner employing non-uniform refractive index distribution," *Opt. Express*, vol. 22, pp. 8533–8540, Apr. 2014

[18] M. R. Paiam, C. F. Janz, R. I. MacDonald, and J. N. Broughton, "Compact planar 980/1550-nm wavelength multi/demultiplexer based on multimode interference," *IEEE Photon. Technol. Lett.*, vol. 7, no. 10, pp. 1180–1182, Oct. 1995.

[19] S.-L. Tsao, H.-C. Guo, and C.-W. Tsai, "A novel 1 × 2 single-mode 1300/1550 nm wavelength division multiplexer with output facet-tilted MMI waveguide," *Opt. Commun.*, vol. 232, pp. 371–379, Mar. 2004.

[20] Q. Deng, L. Liu, X. Li, and Z. Zhou, "Arbitrary-ratio 1×2 power splitter based on asymmetric multimode interference," *Opt. Lett.*, vol. 39, pp. 5590–5593, Oct. 2014.

[21] M. Cherchi, S. Ylinen, M. Harjanne, M. Kapulainen, T. Vehmas, and T. Aalto, "Unconstrained splitting ratios in compact double-MMI couplers," *Opt. Express*, vol. 22, pp. 9245–9253, Apr. 2014.

[22] W. Bogaerts *et al*., "Silicon-on-insulator spectral filters fabricated with CMOS technology," *IEEE J. Sel. Topics Quantum Electron.*, vol. 16, no. 1, pp. 33–44, Jan./Feb. 2010.

[23] B. Shen, P. Wang, R. Polson, and R. Menon, "An integrated-nanophotonics polarization beamsplitter with 2.4 × 2.4 μm^2 footprint," *Nature Photon.*, vol. 9, pp. 378–382, Jun. 2015.

[24] A. Y. Piggott, J. Lu, K. G. Lagoudakis, J. Petykiewicz, T. M. Babinec, and J. Vučković, "Inverse design and demonstration of a compact and broadband on-chip wavelength demultiplexer," *Nature Photon.*, vol. 9, pp. 374–377, 2015.

[25] A. Bakhtazad, J. McMullin, C. Haugen, and R. DeCorby, "MMI multiplexer for dual-channel erbium-doped waveguide amplifiers," *Opt. Express*, vol. 9, pp. 178–183, Aug. 2001.

[26] T. Fujisawa and M. Koshiba, "Full-vector finite-element beam propagation method for three-dimensional nonlinear optical waveguides," *J. Lightw. Technol.*, vol. 20, no. 10, pp. 1876–1884, Oct. 2002.

[27] Y. Jiao, Y. Shi, D. Dai, and S. He, "Accurate and efficient simulation for silicon-nanowire-based multimode interference couplers with a 3D finite-element mode-propagation analysis," *J. Opt. Soc. Amer. B, Opt. Phys.*, vol. 27, pp. 1813–1818, Sep. 2010.

[28] J. Xiao, X. Liu, and X. Sun, "Design of an ultracompact MMI wavelength demultiplexer in slot waveguide structures," *Opt. Express*, vol. 15, pp. 8300–8308, Jun. 2007.

[29] Q. Wang, G. Farrell, and T. Freir, "Effective index method for planar lightwave circuits containing directional couplers," *Opt. Commun.*, vol. 259, pp. 133–136, Mar. 2006.

[30] M. Munowitz and D. J. Vezzetti, "Numerical procedures for constructing equivalent slab waveguides-an alternative approach to effective-index theory," *J. Lightw. Technol.*, vol. 9, no. 9, pp. 1068–1073, Sep. 1991.

[31] N. Ismail, "Integrated Raman spectrometers for applications in health and medicine," Ph.D. dissertation, Elect. Eng., Math. Comput. Sci., Univ. Twente, Enschede, The Netherland, 2012.

[32] L. B. Soldano and E. C. M. Pennings, "Optical multi-mode interference devices based on self-imaging: principles and applications," *J. Lightw. Technol.*, vol. 13, no. 4, pp. 615–627, Apr. 1995.

[33] J. F. Bauters *et al*., "Ultra-low-loss high-aspect-ratio Si_3N_4 waveguides," *Opt. Express*, vol. 19, pp. 3163–3174, Feb. 2011.

Jinfeng Mu received the B.Sc. degree in optical information science and technology from the National University of Defense Technology, Changsha, China, in 2011. Since 2014, he has been working toward the M.Sc. involved Ph.D. program at the Optical Sciences Group, MESA+ Institute for Nanotechnology, University of Twente, The Netherlands. His research interests include optical couplers, photonic integration, and rare-earth-doped waveguide lasers.

Sergio A. Vázquez-Córdova received the Bachelor's degree in physics engineering from the Centro de Investigaciones en Óptica, Universidad de Guanajuato, Guanajuato, Mexico, and the M.Sc. degree from the University of Liverpool, Liverpool, U.K., in 2009. He carried out his master thesis work at the Lairdside Laser Engineering Centre. He is currently working toward the Ph.D. degree at the Optical Sciences Group, MESA+ Institute for Nanotechnology, University of Twente, The Netherlands. After graduating, he joined Solartec, Mexico, where he was a Photovoltaic Support Engineer.

Mustafa Akin Sefunc received the B.Sc. and M.Sc. degrees in electrical and electronics engineering from the Bilkent University, Ankara, Turkey, in 2008 and 2010, respectively. He is currently working toward the Ph.D. degree at the Optical Sciences Group, University of Twente, The Netherlands. His current research interests include developing erbium-doped waveguide amplifiers as well as new fabrication techniques, which make the integration possible on platforms proposed for photonic integration. He received the Optics and Photonics Education Scholarship by SPIE in 2014. He is a Member of IEEE Photonics Society Benelux Chapter and SPIE.

Yean-Sheng Yong received the M.Sc. degree in engineering science from Multimedia University, Malaysia, in 2010. He joined the Faculty of Engineering of Multimedia University as a Lecturer from 2011 to 2012. Since 2012, he has been with the Integrated Optical MicroSystems Group and Optical Sciences Group, MESA+ Institute for Nanotechnology, University of Twente, The Netherlands, carrying out research on rare-earth-doped waveguide amplifiers. His research interests include design and characterization of waveguide amplifiers, integrated photonics devices, as well as III-V active devices.

Sonia M. García-Blanco received the M.Sc. degree from the Universidad Politécnica de Madrid, Madrid, Spain, in 1999 and the Ph.D. degree from the University of Glasgow, Glasgow, U.K., in 2003, for her work on integrated optics for biosensing. She carried out her master thesis work at the IBM Almaden Research Centre, in Almaden, CA, USA. After a two year postdoctoral at the University of Toronto, Toronto, ON, Canada, she joined INO (QC, Canada) as Staff Scientist in 2005. At INO, she led several multidisciplinary projects for several space agencies including the CSA and ESA. She was responsible for the 3-D photonic integration and wafer-level hermetic packaging activities of the company.

In 2010, she joined the University of Twente. She is currently an Associate Professor at the Optical Sciences Group, the MESA+ Institute for Nanotechnology, University of Twente, The Netherlands. Her current research interests include the development of novel active devices integrated as building blocks in passive technology platforms, the use of plasmonics in optical waveguides, and optical sensing based on integrated optics.